crystals

MDPI

Article

Magnesium Coordination Chemistry: A Case Study of Magnesium Carboxylate Complexes with Hexamethylenetetramine

Tomasz Sierański *, Agata Trzęsowska-Kruszyńska *, Marcin Świątkowski, Marta Bogdan and Paulina Sobczak

Institute of General and Ecological Chemistry, Lodz University of Technology, Zeromskiego 116, PL-90924 Lodz, Poland

* Correspondence: tomasz.sieranski@p.lodz.pl (T.S.); agata.trzesowska-kruszynska@p.lodz.pl (A.T.-K.)

Abstract: Three magnesium coordination compounds were obtained to explore the influence of carboxylate anions on the pattern of the formed hydrogen bonds. For their synthesis, various salts of magnesium carboxylic acid (formate, acetate, and propionate) were utilized. As an *N*-donor ligand, hexamethylenetetramine was employed. The supramolecular structures of the obtained compounds were determined and evaluated in Hirshfeld analysis. The length of the carbon chain of the used carboxylate anions has been proven to have a considerable impact on the self-organization of the supramolecular system by altering the three-dimensional net of the created hydrogen bonds. IR spectroscopy was used to characterize the obtained compounds, revealing significant differences between distinct systems. The thermal analysis of the investigated compounds also shows noticeable differences, demonstrating better stability of the systems containing formate anions.

Keywords: magnesium; formate; acetate; propionate; hexamethylenetetramine; crystal structure; thermal analysis; infrared spectroscopy; hydrogen bonds

Citation: Sierański, T.; Trzęsowska-Kruszyńska, A.; Świątkowski, M.; Bogdan, M.; Sobczak, P. Magnesium Coordination Chemistry: A Case Study of Magnesium Carboxylate Complexes with Hexamethylenetetramine. *Crystals* **2022**, *12*, 1434. https://doi.org/10.3390/cryst12101434

Academic Editor: Maria Gazda

Received: 16 September 2022
Accepted: 8 October 2022
Published: 11 October 2022

1. Introduction

The design of the distinctive metal–organic materials attracts growing interest [1–3]. However, synthesizing a solid-state structure with desired properties is a challenging task that demands understanding the influence of many factors, such as characteristics of the used cation, ligands, and solvent(s); and the formation of intermolecular interactions in such a selected environment [4–6]. Currently, the most prevalent strategies that are used in crystal engineering engage hydrogen/halogen-bonding and coordination bonding [7–10]. Achievements in this field contribute to developing many new materials and compounds that might be used, among others, in electronics and the medical and pharmaceutical industries [11–13]. Yet, developing and constructing coordination systems with the requisite topologies and features is still difficult. This requires deep knowledge of the impact of the factors mentioned above on the hierarchy of interactions occurring in the emerging coordination system. One of the cations for which coordination compounds are of interest and for which there is a need for their synthesis is the magnesium cation. The coordination chemistry of this cation is of particular importance due to the unique role of Mg^{2+} in many biological processes [14–17]. At the molecular level, magnesium cations participate in homeostasis, are essential in electrolyte pathophysiology, and activate many enzyme systems such as alkaline phosphatase, peptidases, and enzymes transferring phosphate [18,19]. In addition, enzymes that contribute to vitamin D metabolism are magnesium-dependent [20–22]. Since divalent magnesium is classified as a hard acid, it tends to bind with ligands that contain a hard oxygen atom, such as water molecules or carboxylate, phosphate, and hydroxylate ions. It may be coordinated directly to a macromolecular binding site or indirectly through water molecules. The first type of binding concerns proteins, while binding through coordinating water molecules dominates the interactions with nucleic acids. Even though the coordination chemistry of magnesium is widely explored, the factors that make such systems (including "outer-sphere" coordination mode or "inner-sphere" mode) the

most energetically beneficial are still not fully understood [23–25]. Hence, the investigation of magnesium coordination chemistry, especially related to *N*-donor ligand systems, may help to learn the binding mechanism of this metal to many bioactive molecules (including proteins and nucleic acids) and have vital importance due to the need for biologically active or biologically important magnesium compounds for clinical applications.

In order to broaden the knowledge on crystal engineering of coordination compounds containing an important ion, which is a magnesium cation, a series of its coordination compounds, of general formula $[Mg(H_2O)_6]A_2 \cdot 2$ hmta$\cdot 4H_2O$ (A–carboxylate anion), was obtained. Hexamethylenetetramine (hmta) was selected as an *N*-donor ligand. Carboxylic anions, differing in chain length in each compound, were selected as counterions. Hmta serves as a model ligand for many bioactive molecules (including amino acids, proteins, and nucleotides) due to possessing unshielded nitrogen atoms [26–28]. This ligand also forms many coordination links. It can be present in both the outer and/or inner coordination sphere, where it acts as a bridging and/or terminal ligand [28,29]. Hmta was also a potent agent used for treating urinary tract infections [30]. For all the above reasons, some coordination aspects of the presented magnesium complex compounds can be extended to other bioactive molecules. Additionally, hmta is a vital agent used in the production of powdery or in synthesizing phenolic resins and their molding compounds [31,32]. Usage of modified, hmta-containing compounds as hardening components in these processes can increase the beneficial properties of the mentioned resins. In general, the salts of carboxylic acids are well soluble in water and the carboxylic anions with short carbon chains form associations with water molecules through hydrogen bonds. Using different anions of carboxylic acids (formates, acetates, and propionates) will allow concluding the influence of the length of the carbon chains occurring in these anions on the type of created intermolecular interactions and the geometry of the formed coordination entity. The presented study may be essential not only in obtaining the new materials for potential medical uses, but may also provide further conceptual benefits, and help to understand the relationship between the structure and compound properties (for instance, thermolysis).

2. Materials and Methods

2.1. Materials and Synthesis

All the reagents (hexamethylenetetramine, magnesium carbonate, formic, acetic, and propionic acids) were analytically pure and obtained from POCh S.A (Gliwice, Poland). The samples of magnesium carbonate (0.002 mmol) were suspended in a possibly small amount of water (about 5 cm^3) and then mixed with the formic, acetic, and propionic acid (0.002 mmol), respectively. The mixtures were stirred on a magnetic stirrer for about 15 min, and next, they were filtrated to remove unreacted excess magnesium carbonate. The residues on the filters were washed three times with 5 cm^3 of cold water (the magnesium ions were not detected in the last portion of filtrates). To each solution of combined filtrates (only filtrates relating to the particular magnesium carbonate sample were combined), the 3 cm^3 of a water solution containing 0.1402 g (0.001 mmol) of hmta was added. The obtained solutions were stirred on the magnetic stirrer for 15 min and were placed in a refrigerator at 5 °C. All syntheses were repeated with 1:1 and 1:2 Mg:hmta ratios (0.002 mmol and 0.004 mmol of hmta, respectively). After 3 weeks, the colorless crystals started to grow. The crystals were isolated from the solutions shortly after they were grown. Therefore, a few fractions of crystals were collected from each synthesis solution. The IR spectrum was conducted for each fraction, and the fractions were combined if their spectra were the same. For syntheses performed with 2:1 and 1:1 ratios, the last few fractions were pure magnesium carboxylate salts. Independently of the substrate ratio, the same product was formed for each used magnesium carboxylate. The reaction yields (in relation to hmta), respectively for the syntheses performed with 2:1, 1:1, and 1:2 ratios were: compound 1 (magnesium formate and hmta) 98%, 95%, and 94%; compound 2 (magnesium acetate and hmta) 98%, 94%, and 90%; compound 3 (magnesium propionate and hmta) 97%, 92%, and 89%. Elemental analysis for the obtained compounds 1–3 (calculated/found) [%] (1): C:29.27%/29.21; H:8.01%/7.99%; Mg:4.23%/4.31%;

N:19.50%/19.53%; O:38.99%/39.04; (2): C:31.85%/32,05%; H:8.38%/8.50%; Mg:4.03%/3.89%; N:18.59%/18.71%; O:37.15%/37.01; (3): C:34.28%/34.35; H:8.56%/8.60%; Mg:3.86%/3.77%; N:17.77%/17.89%; O:35.52%/35.60%.

2.2. Crystal Structure Determination

X-ray diffraction data of 1–3 were collected at temperature 291.0(3) K, on a KM-4-CCD automatic diffractometer equipped with CCD detector and fine-focus sealed X-ray tubes generated monochromatic MoK_α and CuK_α radiations. Lorentz, polarization, and numerical absorption [33] corrections were applied. The structures were solved with the SHELXT [34] using intrinsic phasing and refined with the SHELXL [35] using least squares minimization. All the non-hydrogen atoms were refined anisotropically. All the hydrogen atoms were found from the Fourier difference map and refined using the "riding" model. The structure of **2** could not be fully refined due to the disorder of the outer coordination sphere species, which were impossible to localize on the Fourier difference map, despite splitting molecules into parts. The application of the solvent mask function only worsened the refinement. Details concerning crystal data and refinement of **1** and **3** are given in Table 1.

Table 1. Crystal data and structure refinement details for **1** and **3**.

Compound	**1**	**3**
Empirical formula	$C_{14}H_{46}MgN_8O_{14}$	$C_{18}H_{54}MgN_8O_{14}$
Formula weight	574.90	631.00
Crystal system, space group	Triclinic, *P*-1	Triclinic, *P*-1
Temperature (K)	291.0 (3)	291.0 (3)
Radiation	MoKα (λ = 0.71073 Å)	CuKα (λ = 1.54178)
a (Å)	9.2503 (3)	8.3713 (4)
b (Å)	9.2802 (4)	9.1600 (7)
c (Å)	9.3256 (4)	12.0634 (6)
α (°)	76.621 (4)	94.210 (6)
β (°)	60.933 (4)	100.128 (3)
γ (°)	79.673 (3)	114.963 (2)
Volume (Å^3)	678.63 (5)	814.18 (8)
Z, Calculated density (g/cm^3)	1, 1.407	1, 1.287
Absorption coefficient (mm^{-1})	0.142	1.094
Min. and max. transmission	0.946 and 0.968	0.811 and 0.819
F(000)	310	342
Crystal size (mm)	0.381 × 0.299 × 0.267	0.187 × 0.183 × 0.180
2θ range for data collection (°)	4.526 to 50.04	3.77 to 67.64
Index ranges	$-10 \leq h \leq 10$, $-11 \leq k \leq 10$, $-11 \leq l \leq 10$	$-10 \leq h \leq 9$, $-10 \leq k \leq 10$, $-14 \leq l \leq 14$
Reflections collected	6794	9286
Independent reflections	2386 [R_{int} = 0.0202, R_{sigma} = 0.0190]	2800 [R_{int} = 0.0287, R_{sigma} = 0.0275]
Data/restraints/parameters	2386/0/169	2800/0/189
Goodness-of-fit on F^2	1.084	1.059
Final *R* indexes [$I > 2\sigma$ (*I*)]	R_1 = 0.0329, wR_2 = 0.1012	R_1 = 0.0372, wR_2 = 0.0979
Final R indexes [all data]	R_1 = 0.0379, wR_2 = 0.1033	R_1 = 0.0377, wR_2 = 0.0984
Largest diff. peak and hole (e•Å^{-3})	0.47 and −0.19	0.32 and −0.26

2.3. Other Measurements

The thermal analyses were carried out in a TG/DTA-SETSYS-16/18 thermoanalyzer. The samples were heated in corundum crucibles up to 1000 °C at a heating rate of 10 °C min^{-1} in the air atmosphere. Elemental analyses were carried out using a Vario EL III CHNOS elemental analyzer (C, H, N, O). Magnesium content was determined by complexometric titration with the 0.01 mol/dm^3 water EDTA solution as a complexing agent [36]. IR spectra of the investigated compound were recorded as KBr disc on a Nicolet Magna 560 spectrophotometer over the range 4000−400 cm^{-1}.

3. Results and Discussion

3.1. Structural Analysis

The syntheses of magnesium carboxylates (formate, acetate, and propionate) with hmta led to obtaining three coordination compounds of the same formula $[Mg(H_2O)_6]A_2 \cdot 2$ hmta$\cdot 4H_2O$ (A–carboxylate anion). They were formed regardless of the substrate stoichiometry applied in the synthesis reactions. These are discrete compounds with the hexaaquamagnesium coordination entities (Figure 1). In all cases, the central atoms are located on the inversion centers (special positions *h*, *c*, and *e* of the $P2_1$ space group, respectively for **1**–**3**). The coordination polyhedra are almost perfect octahedrons (Table 2). The carboxylate anions are located in the outer coordination sphere together with hmta and water molecules. The Mg:hmta ratio is 1:2. In the case of **2**, the outer coordination sphere species, except hmta, could not be refined due to unsolvable disorder (Figure S1) (see supplementary materials). In consequence, compound 2 was not included in the following structural analysis concerning intermolecular interactions. The composition of **2** was established based on elemental and thermal analyses.

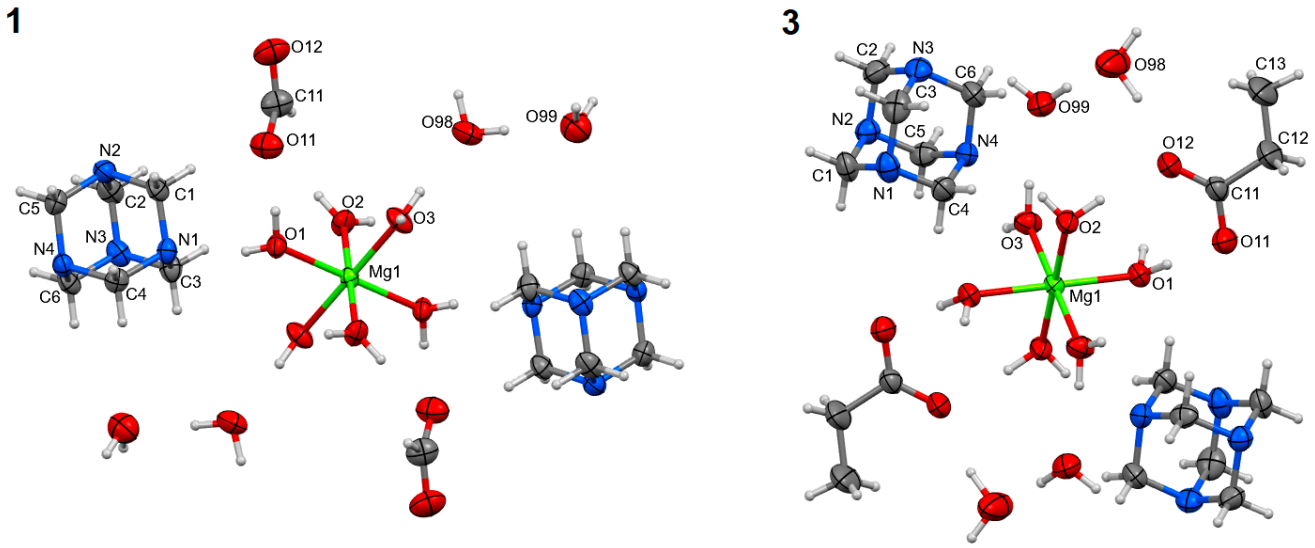

Figure 1. Molecular structures of **1** and **3**, plotted with a 50% probability of displacement ellipsoids of nonhydrogen atoms and as spheres of arbitrary radii for hydrogen atoms. The equivalent atoms (without labels) were generated according to transformation: (**1**) −x + 1, −y + 1, −z + 1; (**3**) −x + 1, −y + 1, −z + 2.

Table 2. Selected structural data for **1** and **3** (Å, °).

Compound 1		**Compound 3**	
Mg1—O1	2.0350 (9)	Mg1—O1	2.0732 (9)
Mg1—O2	2.0695 (10)	Mg1—O2	2.0587 (9)
Mg1—O3	2.0349 (9)	Mg1—O3	2.0716 (9)
O1—Mg1—O2	87.01 (4)	O1—Mg1—O2	90.59 (4)
O1—Mg1—O2 ^{i}	92.99 (4)	O1—Mg1—O2 ^{ii}	89.41 (4)
O1—Mg1—O3	91.06 (4)	O1—Mg1—O3	90.02 (4)
O1—Mg1—O3^{i}	88.94 (4)	O1—Mg1—O3 ^{ii}	89.98 (4)
O2—Mg1—O3	87.93 (4)	O2—Mg1—O3	90.42 (4)
O2—Mg1—O3 ^{i}	92.07 (4)	O2—Mg1—O3 ^{ii}	89.58 (4)

Symmetry transformations used to generate equivalent atoms: (i) −x + 1, −y + 1, −z + 1; (ii) −x + 1, −y + 1, −z + 2.

Despite the same general formula, the supramolecular structures of the studied systems show significant differences. The following hydrogen bonds stabilize their three-dimensional crystal nets: O—H●●●O, O—H●●●N, and C—H●●●O (Table 3). They comprise carboxylate anions, water, and hmta molecules (Figure 2), creating several different

graph set patterns [37,38]. Considering the unitary graph set level, only D motifs are observed. Chain and ring patterns appear in the binary graph set. In the case of **1**, $N_2C_2^2(8)$, $N_2C_4^4(16)$, $N_2R_4^4(12)$, and $N_2R_4^4(16)$ patterns are found. The $C_2^2(8)$ pattern is composed of O1—H1O•••O11 and O2—H2O•••O12 hydrogen bonds, and in this case, the water molecules (acting as hydrogen bond donors) coordinating magnesium ions (each molecule to a different ion) are linked to oxygen atoms of the formate ion (hydrogen bond acceptors). This $C_2^2(8)$ pattern shares the graph paths with the $N_2R_4^4(16)$ ring pattern. One of the $N_2R_4^4(16)$ ring patterns contains coordinated water and hmta molecules linked by O1—H1P•••N1 and O2—H2P•••N4 intermolecular hydrogen bonds. The next two (of a total four) different $N_2R_4^4(16)$ ring patterns also contain hmta molecules. The four existing $N_2C_4^4(16)$ patterns can be expressed as *abba*, *cddc*, *ceec*, and *deed* (where a, b, c, d, and e denote the O1—H1O•••O11, O2—H2O•••O12, O1—H1P•••N1, O2—H2P•••N4, and O3—H3P•••N3 hydrogen bonds, respectively). The solely $N_2R_4^4(12)$ ring is created by O99—H99O•••O11 and O99—H99P•••O12 hydrogen bonds, and it exists between the formate ions and water molecules located in the outer coordination sphere. Unitary graph set level of **3** is created by $C_2^2(8)C_2^2(8)C_2^2(8)R_2^2(8)C_4^4(16)C_4^4(16)C_4^4(16)R_4^4(16)R_4^4(16)R_4^4(16)$ motifs. $C_2^2(8)$, $C_4^4(16)$, and $R_4^4(16)$ patterns are formed by O—H•••N hydrogen bonds between magnesium coordinated water molecules and hmta molecules. $C_2^2(8)$ patterns can be expressed as *ab*, *ac*, and *bc*, whilst $C_4^4(16)$ as *abba*, *acca*, and *bccb* (where a, b, and c refer to O1—H10•••N1, O2—H20•••N4, and O3—H30•••N2 hydrogen bonds, respectively). The same hydrogen bonds create $R_4^4(16)$ patterns and the particular rings can be written as *abab*, *acac*, and *bcbc*. The propionic ions, unlike in **1**, are engaged only in the solely $R_2^2(8)$ pattern created by hydrogen bonds appearing between these ions and magnesium water coordinated molecules (O1—H1P•••O11 and O2—H2P•••O12).

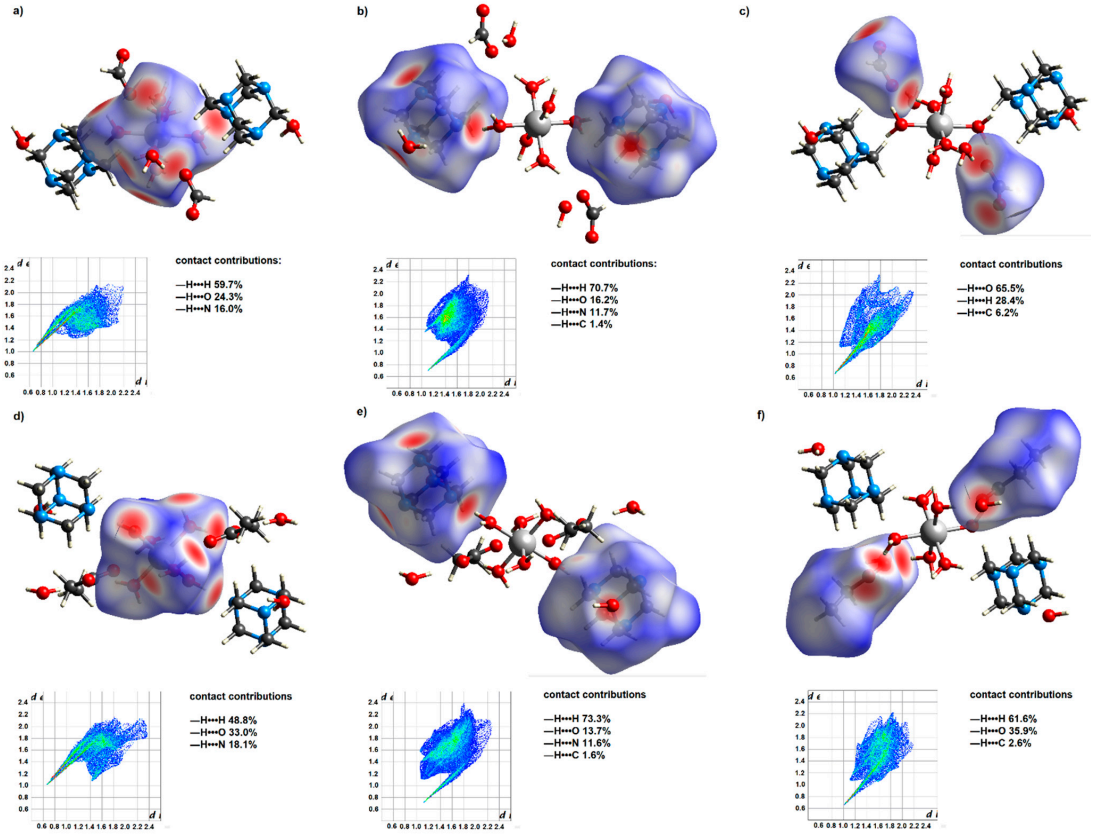

Figure 2. Hirshfeld surfaces of 1 and 3 for their coordination entities (**a**,**d**), hmta ligands (**b**,**e**), and carboxylate anions (**c**,**f**). Two-dimensional fingerprint maps of the mentioned species, together with the contact contributions, are located below the respective surfaces. The Hirshfeld surfaces were plotted over d_{norm}.

Table 3. Hydrogen bonds in **1** and **3** (Å, °).

D-H•••A	d(D-H)	d(H•••A)	d(D•••A)	<(DHA)
Compound 1				
O1—H1O•••O11	0.89	1.80	2.6885(15)	173.5
O1—H1P•••N1 [i]	0.76	2.07	2.8226(15)	166.7
O2—H2O•••O12 [ii]	0.85	1.93	2.7683(16)	169.9
O2—H2P•••N4 [iii]	0.80	2.07	2.8467(15)	164.1
O3—H3O•••O98 [iv]	0.86	1.80	2.6634(14)	173.0
O3—H3P•••N3 [v]	0.88	1.94	2.8182(16)	170.8
O98—H98O•••N2	0.91	1.90	2.8010(16)	174.8
O98—H98P•••O99 [vi]	0.92	1.80	2.7251(18)	177.8
O99—H99O•••O11 [vii]	0.85	1.97	2.7560(18)	154.3
O99—H99P•••O12 [viii]	0.90	1.86	2.729(2)	161.4
Compound 3				
O1—H1O•••N1	0.86	2.00	2.8386(17)	163.6
O1—H1P•••O11 [ix]	0.93	1.75	2.6716(15)	171.6
O2—H2O•••N4 [x]	0.81	2.06	2.8496(18)	163.2
O2—H2P•••O12	0.90	1.81	2.7053(16)	173.0
O3—H3O•••N2 [xi]	0.85	1.98	2.8271(17)	177.4
O3—H3P•••O99 [xii]	0.88	1.89	2.7618(16)	170.0
O98—H98O•••N3 [xiii]	0.91	2.09	2.9609(19)	160.0
O98—H98P•••O12	0.98	1.78	2.751(2)	170.1
O99—H99O•••O11 [xiv]	0.85	1.91	2.756(2)	173.8
O99—H99P•••O98 [xii]	0.93	1.88	2.800(2)	170.0

Symmetry transformations used to generate equivalent atoms: (i) −x + 1, −y + 1, −z + 1; (ii) +x, +y − 1, +z; (iii) +x + 1, +y, +z; (iv) +x, +y + 1, +z; (v) −x + 1, −y + 1, −z; (vi) +x, +y − 1, +z; (vii) +x − 1, +y, +z; (viii) −x + 1, −y + 2, −z; (ix) −x + 1, −y + 1, −z + 2; (x) −x + 1, −y + 2, −z + 2; (xi) x−1, y−1, z; (xii) −x, −y + 1, −z + 1; (xiii) x − 1, y − 1, z − 1; (xiv) −x + 1, −y + 1, −z + 1.

The resulting systems' Hirshfeld surfaces and 2D fingerprints are comparable, yet changes in supramolecular structure may be detected. Such differences demonstrate the influence of the carbon chain length of the present carboxylic acid anions on their participation in the formation of intermolecular interactions. The Hirshfeld surface of the formate anions contains a much greater proportion of the red area (Figure 2), which corresponds to the strong —H•••O interactions. In the case of propionate anions, due to their longer carbon chain, —H•••H contacts account for a more significant contribution to intermolecular interactions. Thus, water molecules of the outer coordination sphere are more actively engaged in creating hydrogen bonds with formate anions. It is reflected in hydrogen bond patterns engaging uncoordinated water molecules and carboxylate anions. In these patterns, the ratio of formate anions to water molecules is 1 to 1, while for propionate anions, it is 1 to 2.

3.2. FT-IR Analysis

The IR spectra of the studied compounds show many similarities (Figures S2–S4). The most noticeable is the strongest band corresponding to the stretching vibration of CN bonds (υ CN) of hmta molecules (Table 4). In the spectra of the coordination compounds, it is slightly shifted towards higher frequencies. Another strong band, corresponding to the NCN bending vibration of hmta (δ NCN), is also shifted toward higher frequencies; however, this shift is stronger (by about 15 cm^{-1}). These shifts are due to the involvement of the nitrogen atoms of the hmta ligand in forming O-H•••N hydrogen bonds that engage water molecules directly coordinated to the magnesium cation. The mentioned band of υ CN and the band assigned to rocking vibrations of CH_2 (ρ CH_2), which serve together to recognize a binding mode of hmta, are not split; thus, confirming uncoordinated hmta [39]. The spectra of all the compounds also contain strong bands corresponding to the asymmetric and symmetric stretching vibrations of the COO groups of carboxylate anions. The difference between their wavenumbers, known as a separation parameter Δυ, is used to

establish the COO coordination behavior [40,41]. For the studied compounds, Δυ is 246, 160, and 141 cm^{-1}. These values are in agreement with those for known compounds containing uncoordinated formate, acetate, and propionate anions [41–43]. The significantly greater value of Δυ for formate, regardless of the same binding mode, results from its different structure. The OCO angle is larger for formate than for acetate and propionate due to a substituent bonded to the COO group (hydrogen versus aliphatic group). It was proven that the larger the OCO angle, the greater Δυ is [41]; thus, Δυ is generally greater for formate than for acetate and propionate. The most significant differences between the spectra of the studied compounds are noted for **1.** Its spectrum contains several weak bands occurring at the wavenumbers in the range of 2700–2800 cm^{-1}. These bands correspond to the stretching vibrations of the CH_2 groups of hmta molecules, and, in the given range, they are not present in the spectra of **2** and **3** (Table 4). Moreover, in the spectrum of **1**, one cannot see a separate band corresponding to the bending vibrations of water molecules. The respective band is seen in the spectra of the other compounds (**2** and **3**) at around 1680 cm^{-1} (Table 4). In the case of all the spectra, the typical broad band associated with the stretching vibrations of the O-H group of water molecules is centered at around 3420–3450 cm^{-1}.

Table 4. Vibrational frequencies (cm^{-1}) and their assignments for the studied compounds.

1	2	3	hmta [44]	$Mg(HCOO)_2$ [45]	$Mg(CH_3COO)_2$ [46]	$NaCH_3CH_2COO$ [43]	Assignment
3427 br	3444 br	3422 br					υ OH (H_2O)
2975 w	2974 w	2977 w	2966			2973	$υ_{as}$ CH_2, $υ_{as}$ CH_3
2937 w	2938 w	2941 w	2955	2907	2930	2937	$υ_s$ CH_2, υ CH, $υ_s$ CH_3
	2891 w	2888 w	2874				$υ_s$ CH_2
2796 w							$υ_s$ $CH_2(NCH_2N)$
2742 w							$υ_s$ $CH_2(NCH_2N)$
2719 w							$υ_s$ $CH_2(NCH_2N)$
2477 w	2477 w	2477 w					$υ_s$ $CH_2(NCH_2N)$
	1683 m	1679 m					δ OH (H_2O)
1596 s	1568 s	1558 s		1615	1554	1563	$υ_{as}$ COO
1466 m	1464 s	1465 s	1458		1450	1461	σ CH_2, $δ_{as}$ CH_3
	1408 s	1417 s			1430	1428	$υ_s$ COO
1383 s	1380 m	1379 m	1370	1392		1376	ω CH_2, δ-α CH, $δ_s$ CH_3
1350 s				1365			$υ_s$ COO
	1343 w				1351		$δ_s$ CH_3
		1299 s				1301	ω CH_2
1241 s	1240 s	1240 s	1234				ρ CH_2
		1078 w				1077	ρ-α CH_3
1009 s	1010 s	1010 s	1007				υ CN
	924 m	877 w			949	881	υ CC
814 m	814 w	817 w	825				υ CN
765 m	752 br	758 br		761	671	646	σ COO
688 s	687 s	690 s	673				δ NCN
508 m	507 m	509 m	512				ω NCN

Vibrations symbols: w—weak, m—medium, s—strong, br—broadened, υ—stretching, δ—bending, τ—twisting, ω—wagging, σ—scissoring, ρ—rocking, α—in-plane, γ—out-of-plane, s—symmetric, as—asymmetric.

3.3. Thermal Analysis

The thermal decomposition of the studied compounds is a gradual process (Figures S5–S7). In the case of all the compounds, the first state is associated with the endothermic removal of water molecules. In **1** and **3**, this is a one-step process; in 2 at the beginning, only water molecules of the outer coordination sphere are lost. The mass loss indicates four water molecules, which next to elemental analysis, is an additional confirmation of the water content in **2** (Table 5)**.** The six remaining water molecules (belonging to the inner coordination sphere) are removed during the second stage. At this point, the mass spectra show ion current signals m/z = 17 and m/z = 18, which correspond to the OH^+ and H_2O^+ species. The second stage of thermal decomposition is the removal of hmta molecules. At the beginning, the hmta is lost during its sublimation, as indicated by an endothermic process registered on DTA curves (Figures S5–S7), as well as the most characteristic fragmentation ions of hmta; i.e., $C_2H_4N^+$ (m/z = 42) is detected in the mass spectra. As the decomposition continues, the non-sublimated hmta molecules are

combusted, and the mass spectrum shows ion current signals corresponding to C^+, N^+, OH^+, H_2O^+, CO^+, NO^+, and CO_2^+ species. For **2** and **3**, the carboxylate anions decompose before the hmta degradation is completed (third stage). The mass spectra show the same ion current signal as stated above (excluding m/z = 42). In all cases, the process finishes with the formation of magnesium oxide as the final product.

Table 5. Thermal analysis data: temperature ranges, DTA extrema (exo—exothermic, endo—endothermic), mass losses (experimental/calculated), and mz/signals; for the studied compounds.

	1	**2**	**3**	***m*/*z***
I stage	120–202 °C, 135 °C endo 31.6%/31.3% −10 H_2O	43–132 °C, 90 °C endo 11.8%/11.9% −4 H_2O	45–133 °C, 90 °C endo 26.8%/28.5% −10 H_2O	17, 18
II stage	202–313 °C, 250 °C endo 48.4%/48.7% −2 hmta	132–278 °C, 215 °C endo 59.1%/−	133–260 °C, 225 °C endo 38.6%/−	12, 14, 17, 18, 30, 42, 44
III stage	313–423 °C, 380 °C exo 12.9%/12.9% −2 $HCOO^-$, +0.5 O_2	278–450 °C, 315 °C exo, 355 °C exo 22.2%/−	260–455 °C, 305 °C endo, 365 °C exo 28.1%/−	12, 14 *, 17, 18, 30 *, 44
		II and III stages totally: 81.3%/81.4% −6 H_2O, −2 hmta, −2 CH_3COO^-, +0.5 O_2	II and III stages totally: 66.7%/65.0% −2 hmta, −2 $C_2H_5COO^-$, +0.5O_2	
Final product	7.1 %/7.1% MgO	6.9%/6.7% MgO	6.5%/6.5% MgO	-

* m/z signals present only in the thermal decomposition of **2** and **3**.

4. Conclusions

The studied compounds were formed regardless of the applied substrate stoichiometry during the synthesis. The location of the hmta molecules in the outer coordination sphere and the presence of $Mg(H_2O)_6^{2+}$ ions are beneficial for the optimal pharmaceutical activity of both species. Due to the uncoordinated nature of the carboxylate ions, which contrasts with the majority of magnesium carboxylate complexes, the studied compounds are structurally uncommon [47]. The carbon chain length of the carboxylate anions is a key factor in supramolecular assembling. In the studied systems, the propioniate anions engage twice as many water molecules of the outer coordination sphere to form hydrogen bonds as do formate anions. Thus, a slight change in the carbon chain length significantly affects the type of created supramolecular interactions. This, in turn, considerably affects the thermal stability of the investigated compounds. The compound containing formate anions occurred to be notably more thermally stable.

Supplementary Materials: The following supporting information can be downloaded at: https://www.mdpi.com/article/10.3390/cryst12101434/s1, Figure S1: Unit cell of 2 showing the unsolvable disorder in the outer coordination sphere title; Figures S2–S4: IR spectra of 1–3; Figures S5–S7: TG and DTA curves of 1–3.

Author Contributions: Conceptualization, T.S. and A.T.-K.; investigation, visualization, T.S., M.Ś., M.B. and P.S.; writing—original draft preparation, T.S., A.T.-K. and M.Ś.; writing—review and editing, M.Ś., M.B. and P.S.; supervision, T.S. and A.T.-K. All authors have read and agreed to the published version of the manuscript.

Funding: This research received no external funding.

Institutional Review Board Statement: Not applicable.

Informed Consent Statement: Not applicable.

Data Availability Statement: CCDC 2207826 and 2207827 contain the supplementary crystallographic data for 1 and 3. These data can be obtained free of charge via http://www.ccdc.cam.ac.uk/conts/retrieving.html (accessed on 16 September 2022) or from the CCDC, 12Union Road, Cambridge CB2 1EZ, UK (fax: +44−1223−336033; e-mail: deposit@ccdc.cam.ac.uk).

Acknowledgments: This article has been completed while the fifth author (Paulina Sobczak) was the Doctoral Candidate in the Interdisciplinary Doctoral School at the Lodz University of Technology, Poland.

Conflicts of Interest: The authors declare no conflict of interest.

References

1. Koroteev, P.S.; Ilyukhin, A.B.; Gavrikov, A.V.; Babeshkin, K.A.; Efimov, N.N. Mononuclear Transition Metal Cymantrenecarboxylates as Precursors for Spinel-Type Manganites. *Molecules* **2022**, *27*, 1082. [CrossRef] [PubMed]
2. Krejner, E.; Sierański, T.; Świątkowski, M.; Bogdan, M.; Kruszyński, R. Physicochemical Insight into Coordination Systems Obtained from Copper(II) Bromoacetate and 1,10-Phenanthroline. *Molecules* **2020**, *25*, 5324. [CrossRef] [PubMed]
3. Liu, J.; Xie, D.; Xu, X.; Jiang, L.; Si, R.; Shi, W.; Cheng, P. Reversible Formation of Coordination Bonds in Sn-Based Metal-Organic Frameworks for High-Performance Lithium Storage. *Nat. Commun.* **2021**, *12*, 3131. [CrossRef] [PubMed]
4. Malinowski, J.; Zych, D.; Jacewicz, D.; Gawdzik, B.; Drzeżdżon, J. Application of Coordination Compounds with Transition Metal Ions in the Chemical Industry—A Review. *Int. J. Mol. Sci.* **2020**, *21*, 5443. [CrossRef] [PubMed]
5. Seetharaj, R.; Vandana, P.V.; Arya, P.; Mathew, S. Dependence of Solvents, PH, Molar Ratio and Temperature in Tuning Metal Organic Framework Architecture. *Arab. J. Chem.* **2019**, *12*, 295–315. [CrossRef]
6. Chen, X.-M. Chapter 10-Assembly Chemistry of Coordination Polymers. In *Modern Inorganic Synthetic Chemistry*; Xu, R., Pang, W., Huo, Q., Eds.; Elsevier: Amsterdam, The Netherlands, 2011; pp. 207–225, ISBN 978-0-444-53599-3.
7. Mukherjee, A.; Tothadi, S.; Desiraju, G.R. Halogen Bonds in Crystal Engineering: Like Hydrogen Bonds yet Different. *Acc. Chem. Res.* **2014**, *47*, 2514–2524. [CrossRef]
8. Biradha, K. Crystal Engineering: From Weak Hydrogen Bonds to Co-Ordination Bonds. *CrystEngComm* **2003**, *5*, 374–384. [CrossRef]
9. Desiraju, G.R. Crystal Engineering: A Holistic View. *Angew. Chem. Int. Ed. Engl.* **2007**, *46*, 8342–8356. [CrossRef]
10. Metrangolo, P.; Resnati, G.; Pilati, T.; Liantonio, R.; Meyer, F. Engineering Functional Materials by Halogen Bonding. *J. Polym. Sci. Part A Polym. Chem.* **2007**, *45*, 1–15. [CrossRef]
11. Wang, H.-N.; Meng, X.; Dong, L.-Z.; Chen, Y.; Li, S.-L.; Lan, Y.-Q. Coordination Polymer-Based Conductive Materials: Ionic Conductivity vs. Electronic Conductivity. *J. Mater. Chem. A* **2019**, *7*, 24059–24091. [CrossRef]
12. Gul, Z.; Khan, S.; Ullah, S.; Ullah, H.; Khan, M.U.; Ullah, M.; Altaf, A.A. Recent Development in Coordination Compounds as a Sensor for Cyanide Ions in Biological and Environmental Segments. *Crit. Rev. Anal. Chem.* 2022, 1–21, *online ahead of print*. [CrossRef]
13. Medici, S.; Peana, M.; Crisponi, G.; Nurchi, V.M.; Lachowicz, J.I.; Remelli, M.; Zoroddu, M.A. Silver Coordination Compounds: A New Horizon in Medicine. *Coord. Chem. Rev.* **2016**, *327–328*, 349–359. [CrossRef]
14. Yamagami, R.; Sieg, J.P.; Bevilacqua, P.C. Functional Roles of Chelated Magnesium Ions in RNA Folding and Function. *Biochemistry* **2021**, *60*, 2374–2386. [CrossRef] [PubMed]
15. Rezaei Behbehani, G.; Saboury, A.A. A Thermodynamic Study on the Binding of Magnesium with Human Growth Hormone. *J. Anal. Calorim.* **2007**, *89*, 857–861. [CrossRef]
16. Grubbs, R.D.; Maguire, M.E. Magnesium as a Regulatory Cation: Criteria and Evaluation. *Magnesium* **1987**, *6*, 113–127.
17. Ayuk, J.; Gittoes, N.J. Contemporary View of the Clinical Relevance of Magnesium Homeostasis. *Ann. Clin. Biochem* **2014**, *51*, 179–188. [CrossRef]
18. Mildvan, A.S. Role of Magnesium and Other Divalent Cations in ATP-Utilizing Enzymes. *Magnesium* **1987**, *6*, 28–33.
19. Jahnen-Dechent, W.; Ketteler, M. Magnesium Basics. *Clin. Kidney J.* **2012**, *5*, i3–i14. [CrossRef]
20. Uwitonze, A.M.; Razzaque, M.S. Role of Magnesium in Vitamin D Activation and Function. *J. Am. Osteopath Assoc.* **2018**, *118*, 181–189. [CrossRef]
21. Gong, R.; Liu, Y.; Luo, G.; Yang, L. Dietary Magnesium Intake Affects the Vitamin D Effects on HOMA-β and Risk of Pancreatic β-Cell Dysfunction: A Cross-Sectional Study. *Front. Nutr.* **2022**, *9*, 849747. [CrossRef]
22. Dai, Q.; Zhu, X.; Manson, J.E.; Song, Y.; Li, X.; Franke, A.A.; Costello, R.B.; Rosanoff, A.; Nian, H.; Fan, L.; et al. Magnesium Status and Supplementation Influence Vitamin D Status and Metabolism: Results from a Randomized Trial. *Am. J. Clin. Nutr* **2018**, *108*, 1249–1258. [CrossRef]
23. Petrov, A.S.; Pack, G.R.; Lamm, G. Calculations of Magnesium−Nucleic Acid Site Binding in Solution. *J. Phys. Chem. B* **2004**, *108*, 6072–6081. [CrossRef]
24. Dudev, T.; Cowan, J.A.; Lim, C. Competitive Binding in Magnesium Coordination Chemistry: Water versus Ligands of Biological Interest. *J. Am. Chem. Soc.* **1999**, *121*, 7665–7673. [CrossRef]
25. Piovesan, D.; Profiti, G.; Martelli, P.L.; Casadio, R. The Human "Magnesome": Detecting Magnesium Binding Sites on Human Proteins. *BMC Bioinform.* **2012**, *13*, S10. [CrossRef] [PubMed]

26. Sieranski, T.; Kruszynski, R. Magnesium Sulphate Complexes with Hexamethylenetetramine and 1,10-Phenanthroline. *J. Anal. Calorim* **2012**, *109*, 141–152. [CrossRef]
27. Yufanyi, D.M.; Ondoh, A.M.; Foba-Tendo, J.; Mbadcam, K.J. Effect of Decomposition Temperature on the Crystallinity of α-Fe_2O_3 (Hematite) Obtained from an Iron(III)-Hexamethylenetetramine Precursor. *Am. J. Chem.* **2015**, *5*, 1–9.
28. Kirillov, A.M. Hexamethylenetetramine: An Old New Building Block for Design of Coordination Polymers. *Coord. Chem. Rev.* **2011**, *255*, 1603–1622. [CrossRef]
29. Czubacka, E.; Kruszynski, R.; Sieranski, T. The Structure and Thermal Behaviour of Sodium and Potassium Multinuclear Compounds with Hexamethylenetetramine. *Struct. Chem.* **2012**, *23*, 451–459. [CrossRef]
30. Chwa, A.; Kavanagh, K.; Linnebur, S.A.; Fixen, D.R. Evaluation of Methenamine for Urinary Tract Infection Prevention in Older Adults: A Review of the Evidence. *Adv. Drug Saf.* **2019**, *10*, 2042098619876749. [CrossRef]
31. Hirano, K.; Asami, M. Phenolic Resins—100 years of Progress and Their Future. *React. Funct. Polym.* **2013**, *73*, 256–269. [CrossRef]
32. Choi, M.H.; Chung, I.J.; Lee, J.D. Morphology and Curing Behaviors of Phenolic Resin-Layered Silicate Nanocomposites Prepared by Melt Intercalation. *Chem. Mater.* **2000**, *12*, 2977–2983. [CrossRef]
33. STOE & Cie GmbH. *X-RED Version 1.18*; STOE & Cie GmbH: Darmstadt, Germany, 1999.
34. Sheldrick, G.M. SHELXT–Integrated Space-Group and Crystal-Structure Determination. *Acta Cryst. A* **2015**, *71*, 3–8. [CrossRef] [PubMed]
35. Sheldrick, G.M. Crystal Structure Refinement with SHELXL. *Acta Cryst. C* **2015**, *71*, 3–8. [CrossRef] [PubMed]
36. Welcher, F.J. *Analityczne Zastosowanie Kwasu Wersenowego (Eng. The Analytical Uses of Etylenediamineteraacetic Acid)*; WNT: Warsaw, Poland, 1963.
37. Bernstein, J.; Davis, R.E.; Shimoni, L.; Chang, N.-L. Patterns in Hydrogen Bonding: Functionality and Graph Set Analysis in Crystals. *Angew. Chem. Int. Ed. Engl.* **1995**, *34*, 1555–1573. [CrossRef]
38. Shimoni, L.; Glusker, J.P.; Bock, C.W. Energies and Geometries of Isographic Hydrogen-Bonded Networks. 1. The (8) Graph Set. *J. Phys. Chem.* **1996**, *100*, 2957–2967. [CrossRef]
39. Ahuja, I.S.; Singh, R.; Yadava, C.L. Infrared Spectral Evidence for Mono-, Bi- and Tetra-Dentate Behaviour of Hexamethylenetetramine. *Proc. Indian Acad. Sci. (Chem. Sci.)* **1983**, *92*, 59–63. [CrossRef]
40. Deacon, G.B.; Phillips, R.J. Relationships between the Carbon-Oxygen Stretching Frequencies of Carboxylato Complexes and the Type of Carboxylate Coordination. *Coord. Chem. Rev.* **1980**, *33*, 227–250. [CrossRef]
41. Sutton, C.C.R.; da Silva, G.; Franks, G.V. Modeling the IR Spectra of Aqueous Metal Carboxylate Complexes: Correlation between Bonding Geometry and Stretching Mode Wavenumber Shifts. *Chem.–A Eur. J.* **2015**, *21*, 6801–6805. [CrossRef]
42. Swiatkowski, M.; Kruszynski, R. Structurally Diverse Coordination Compounds of Zinc as Effective Precursors of Zinc Oxide Nanoparticles with Various Morphologies. *Appl. Organomet. Chem.* **2019**, *33*, e4812. [CrossRef]
43. Kakihana, M.; Akiyama, M. Vibrational Analysis of the Propionate Ion and Its Carbon-13 Derivatives: Infrared Low-Temperature Spectra, Normal-Coordinate Analysis, and Local-Symmetry Valence Force Field. *J. Phys. Chem.* **1987**, *91*, 4701–4709. [CrossRef]
44. Jensen, J.O. Vibrational Frequencies and Structural Determinations of Hexamethylenetetraamine. *Spectrochim. Acta A Mol. Biomol. Spectrosc.* **2002**, *58*, 1347–1364. [CrossRef]
45. Stoilova, D.; Koleva, V. IR Study of Solid Phases Formed in the Mg(HCOO)2–Cu(HCOO)2–H2O System. *J. Mol. Struct.* **2000**, *553*, 131–139. [CrossRef]
46. Koleva, V.; Stoilova, D. Infrared and Raman Studies of the Solids in the Mg(CH3COO)2–Zn(CH3COO)2–H2O System. *J. Mol. Struct.* **2002**, *611*, 1–8. [CrossRef]
47. Groom, C.R.; Bruno, I.J.; Lightfoot, M.P.; Ward, S.C. The Cambridge Structural Database. *Acta Cryst. B* **2016**, *72*, 171–179. [CrossRef] [PubMed]